A sensitivity analysis of kinetic characterizations in continuous flotation circuits under moderate deviations with respect to perfect mixing

Luis Vinnett[1], Catalina A. Pino-Muñoz[2], Juan Yianatos[1], Francisco Díaz[3], Felipe Henríquez[4]

[1] Department of Chemical and Environmental Engineering, Universidad Técnica Federico Santa María, Valparaíso, Chile

[2] Department of Earth Science and Engineering, Imperial College London, London, United Kingdom

[3] Trazado Nuclear e Ingeniería, Santiago, Chile

[4] Minera Los Pelambres, Antofagasta Minerals, Salamanca, Chile

Corresponding author: luis.vinnett@usm.cl (Luis Vinnett)

Abstract: This paper studies the effect of moderate deviations with respect to perfect mixing on the estimated kinetic parameters in industrial flotation banks. Radioactive tracer tests and mass balance surveys were performed to characterize the mixing regimes and Cu kinetic responses. For three models (Single Rate Constant, Rectangular and Gamma), two approaches to incorporate the residence time distributions (RTD) in the kinetic characterizations of rougher banks were compared: (i) RTDs measured from the radioactive tracer tests; and (ii) pure perfect mixing in each flotation machine. The measured RTDs did not present significant bypass in the evaluated banks. In all cases, comparable model fitting was obtained with both RTD approaches, which indicates that the kinetic models add sufficient flexibility to compensate for moderate biases in the mixing regime. The studied kinetic models showed non-significant differences in the estimated maximum recoveries (R_∞), mean (k_{mean}) and median (k_{50}) rate constants when comparing the process modelling from measured RTDs and pure perfect mixing. However, the Gamma model was more sensitive to the RTD assumption in terms of the shapes of the flotation rate distributions. From the results, kinetic characterizations focused only on model fitting, or on R_∞ and k_{mean} (or k_{50}) estimations have low sensitivity to the assumption of perfect mixing when the RTDs present moderate deviations with respect to this regime. Special attention must be paid when characterizing floating components as the perfect mixing assumption may bias the shapes of the flotation rate distributions.

Keywords: flotation kinetics, residence time distribution, perfect mixing, flotation rate distribution, industrial flotation circuit

1. Introduction

Flotation kinetics has been object of extensive literature due to its significant impact on the metallurgical performance at laboratory, pilot, and industrial scales. Comprehensive overviews on this topic have been reported by Huber-Panu *et al.* (1976), Ek (1992), Gharai and Venugopal (2016), Bu *et al.* (2017b), just to name a few. García-Zuniga (1935) described kinetic responses in batch flotation as first-order rate processes. From different ores, the mineral concentrations showed exponential decays over time, reaching plateaus at the end of the tests. As a result, the mineral recovery R as a function of time t was described by $R(t) = R_\infty [1 - \exp(-k\,t)]$, with k denoting the flotation rate constant and R_∞ the maximum recovery. Schuhmann (1942) determined rate constants in a continuous lab-scale flotation cell, assuming $R_\infty = 100$.

From batch tests, Imaizumi and Inoue (1963) identified non-linearity in the flotation rates, which led to deviations with respect to first-order decays. Two possible causes for this phenomenon were discussed: (i) interactions between flotation mechanisms; and (ii) a distribution of flotation rates that were related to the wide range of particle properties. Imaizumi and Inoue (1963) indicated that the

flotation rate is not constant but variant, introducing a spectrum of rate constants or flotation rate distribution $f(k)$. Thus, the batch flotation process was expressed as a continuous sum of exponential decays. Discrete or continuous flotation rate distributions have been empirically justified by the heterogeneous kinetic responses by size (Yekeler and Sönmez, 1997; Abkhoshk *et al.*, 2010; Bu *et al.*, 2017a) and by other particle properties (Polat and Chander, 2000; Vinnett *et al.*, 2021). Several studies have detailed, evaluated and compared different model structures for $f(k)$ (Dowling *et al.*, 1985; Polat and Chander, 2000; Ai *et al.*, 2017; Bu *et al.*, 2017b; Vinnett and Waters, 2020), showing their advantages with respect to single rate constants.

Woodburn and Loveday (1965) studied the metallurgical performance of a continuous flotation cell in terms of $f(k)$ and the residence time distribution $h(t)$. The mineral concentration C that is rejected to the tailings was expressed by Eq. (1).

$$C = C_\infty \int_0^\infty \int_0^\infty \exp(-k\,t)\,f(k)h(t)\,dk\,dt \tag{1}$$

where C_∞ is the mineral concentration at $t \to \infty$.

Woodburn and Loveday (1965) measured residence time distributions (RTD) in a 1 ft³ cell, obtaining conditions close to perfect mixing. A Gamma $f(k)$ was also chosen to describe the rate process, while perfect mixing was assumed for the pulp $h(t)$. From Eq. (1), Eq. (2) is obtained for the collection zone recovery. Equation (2) has also been used for overall flotation kinetics, in which $f(k)$ represents an apparent flotation rate distribution. Woodburn and Loveday (1965) presented the fraction of mineral recovered into the concentrate stream by parametric graphs.

$$R = R_\infty \int_0^\infty \int_0^\infty [1 - \exp(-k\,t)]\,f(k)h(t)\,dk\,dt \tag{2}$$

Given a model structure for the residence time distribution, Eq. (2) allows for a variety of kinetic models in continuous flotation systems, from different $f(k)$s. Typically, apparent rate constants are assumed in $f(k)$, which implicitly incorporate froth recoveries. Otherwise, Eq. (2) only describes the collection zone recovery and froth recoveries must be measured throughout the flotation circuit to characterize the flotation process. Kinetic modelling in continuous flotation circuits commonly assumes a single (deterministic) rate constant or a Rectangular $f(k)$, together with perfect mixing in each flotation cell (Védrine *et al.*, 1991; Qaredaqi *et al.*, 2012; Boeree, 2014; Saldaña *et al.*, 2021). Both assumptions simplify the mathematical treatment and allow the typically unknown $h(t)$ to be available. However, the impact of this $h(t)$ assumption on kinetic characterizations has not been discussed in flotation literature.

This paper evaluates the impact of moderate $h(t)$ deviations with respect to perfect mixing on the R_∞ - $f(k)$ estimates, in which $f(k)$ describes apparent flotation rates. The study is supported by RTD measurements and kinetic characterizations in two industrial-scale flotation banks.

2.   Materials and methods

2.1. Industrial data

A sampling survey was conducted at Minera Los Pelambres concentrator, which involved hydrodynamic and metallurgical characterizations. Residence time distributions and flotation kinetics were estimated in a rougher flotation circuit. A schematic of this circuit is presented in Fig. 1. The studied stage consisted of three parallel flotation banks (A, B and C). The survey was performed in the rougher banks A and B. Bank A consists of nine 130 m³ Wemco cells in a 1-2-2-2-2 arrangement, whereas bank B consists of six 250 m³ Dorr-Oliver Eimco cells in a 1-1-1-1-1-1 arrangement. From mass balances, the rougher bank A was fed with approximately 600 tph of a copper ore and Cu feed grade of 0.86%. The rougher bank B was fed with approximately 700 tph of solid and Cu feed grade of 0.70%.

RTD measurements were carried out using the radioactive tracer technique. The injection (green squares) and detection (red diamonds) points are depicted in Fig. 1. The tracer was injected into the feed distributor, and the tracer detectors were installed throughout the rougher banks A and B. In bank A, the detectors were placed at the feed of cell 1 and tailings of cells 1, 3, 5, 7 and 9. In bank B, the detectors were placed at the feed of cell 1 and the tailings of each flotation cell. Irradiated non-floatable solid from the rougher tailings was employed as a tracer to ensure similar physical and chemical properties to that of the fed material. The irradiation was conducted in a thermal 5 MW reactor, using a neutronic flux of

up to 5×10^{13} n cm^{-2} s^{-1}, spatially homogeneous in 4π. The samples were placed inside a grid with the combustible elements exposed to this flux for approximately 20 h. All samples were activated at the nuclear reactor of the Chilean Commission of Nuclear Energy, in Santiago, Chile. Radioactivity type and intensity were determined, taking the flow rates and pulp characteristics into consideration for real-time measurements. Tracer activities were calculated to provide enough significance (*ca.*, 50 times) above the typical local background (*i.e.*, 10–20 cps). The mean tracer lifetime was approximately 15 h. A hydraulic injection system was used to produce an almost instantaneous, simple, and safe tracer injection. Tracer concentrations were measured as activity at each detection point. Onstream non-invasive sensors, scintillating crystal of 1"x1.5" NaI(Tl) (Saphymo, France), were employed for data acquisition. All data were corrected by radioactive decay and local radiation background, and then normalized for comparison purposes. Fig. 2 illustrates inlet and outlet tracer concentrations in the rougher bank A.

Twenty-six streams were sampled for the kinetic characterization of banks A and B (black circles in Fig. 1). For the rougher bank A, 12 streams were sampled to estimate the recoveries in each arrangement, in the first cell, and in the overall bank. For the rougher bank B, 14 streams were sampled to estimate the recoveries in each flotation cell, and in the overall bank. Each sample was a composite of approximately 20 L, which was taken every 30 min, for 2 hours, to account for approximately four times the mean residence time of the circuit. All samples were assayed for copper (Cu), molybdenum (Mo) and iron (Fe). Only Cu recoveries consistently approached a plateau at the end of the banks, which allowed the maximum recoveries to be bounded. Data reconciliation was performed to satisfy all mass balances, minimizing relative differences between the measured and reconciled grades (Wills and Napier-Munn, 2006; Vinnett *et al*, 2016). As a result, adjusted Cu recoveries and grade profiles were obtained in the rougher banks. From the experimental t – R(t) data and Eq. (2), the R_∞ - $f(k)$ pairs were estimated for Cu by non-linear regression, given an experimental RTD and a model structure for the kinetic response.
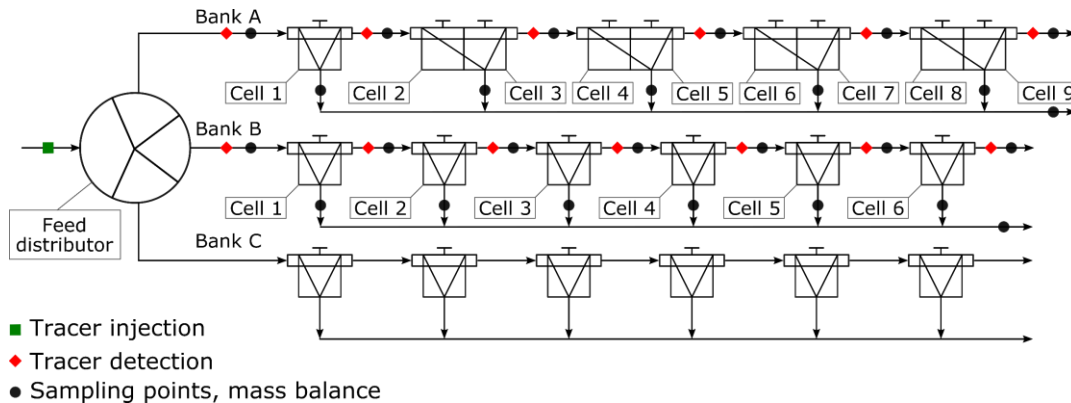

Fig. 1. Schematic of the rougher circuit depicting the radioactive tracer injection (green squares) and detection (red diamonds) points, and the sampling points in the mass balances (black circles)
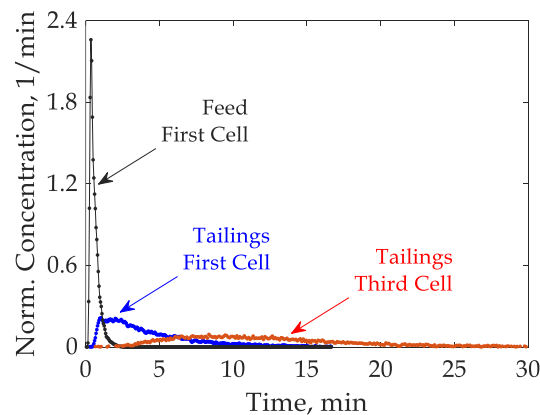

Fig. 2. Examples of normalized tracer concentrations, rougher bank A

2.2. Modelling Residence Time Distributions

The residence time distributions were estimated by a parametric deconvolution methodology (Yianatos *et al.*, 2015). Given measured inlet [$x(t)$] and outlet [$y(t)$] tracer concentrations and a model structure for the RTDs [$h(t)$], Eq. (3) allowed the RTD parameters to be obtained by minimizing the squared reconstruction errors for the outlet concentrations:

$$\min \ \sum[y(t) - x(t) * h(t)]^2 \tag{3}$$

Within Eq. (3)* denotes convolution. The optimization problem of Eq. (3) was solved in Matlab, using the Optimization Toolbox (The MathWorks, USA).

For single flotation cells (*i.e.*, first flotation cells), three model structures for the residence time distribution were evaluated: (i) a single perfect mixer; (ii) two parallel perfect mixers; and (iii) a large perfect mixer in series with a small perfect mixer [Large and Small Tanks in Series (LSTS) model]. In all three models, a transport delay (τ_D) was incorporated. In the absence of this transport delay, these model structures led to poor model fitting. Table 1 summarizes the studied RTD models for single cells, the respective mean residence times (τ_{mean}) and the equation numbers. For the first cell of each rougher bank, the best $h(t)$ model was chosen in terms of the adjusted coefficient of determination.

Table 1. Model structures for residence time distributions in single flotation cells

Model	$h(t)$	τ_{mean}	Equation Numbers
Perfect Mixer + Transport Delay (*)	$\dfrac{1}{\tau_{PM}}\exp\left(-\dfrac{t-\tau_D}{\tau_{PM}}\right), \ t > \tau_D$	$\tau_{PM} + \tau_D$	(4)
Two Parallel Perfect Mixers + Transport Delay (**)	$\dfrac{\alpha}{\tau_1}\exp\left(-\dfrac{t-\tau_D}{\tau_1}\right) +$ $\dfrac{(1-\alpha)}{\tau_2}\exp\left(-\dfrac{t-\tau_D}{\tau_2}\right), \ t > \tau_D$	$\alpha\,\tau_1 + (1-\alpha)\,\tau_2 + \tau_D$	(5)
Large and Small Tanks in Series + Transport Delay (***)	$\dfrac{1}{(\tau_L - \tau_S)}\left[\exp\left(-\dfrac{t-\tau_D}{\tau_L}\right) + \exp\left(-\dfrac{t-\tau_D}{\tau_S}\right)\right], \ t > \tau_D$	$\tau_L + \tau_S + \tau_D$	(6)

(*) τ_{PM} corresponds to the residence time of a perfect mixer; (**) α corresponds to the fraction that is fed to a perfect mixer with residence time τ_1, whereas its complement is fed to a perfect mixer with residence time τ_2; (***) τ_L and τ_S correspond to the residence times of the large and small perfect mixers, respectively.

For arrangements of cells in series, the N perfectly-mixed-reactors-in-series model of Eq. (7) was employed to represent the RTDs:

$$h(t) = \frac{(t-\tau_D)^{N-1}}{\tau_M^N \Gamma(N)} \exp\left[-\frac{(t-\tau_D)}{\tau_M}\right], \ t \geq \tau_D, \ \tau_{mean} = N\tau_M + \tau_D \tag{7}$$

where N corresponds to the number of equivalent perfect mixers in series, τ_M to the residence time of a single perfect mixer and $\Gamma(N)$ to the Gamma function. A transport delay was again incorporated to adequately fit the experimental data.

From the objective function of Eq. (3) and the model structures of Eqs. (4) to (7) the estimated RTDs were obtained. These RTDs were used to characterize the kinetic responses [Eq. (2)] throughout the rougher banks. These responses were also modelled, assuming pure perfect mixing with a mean residence time τ_{PPM} in each flotation machine, as typically reported in literature. Thus, for single flotation cells, Eq. (8) was evaluated.

Similarly, for arrangements of cells in series, the N perfectly-mixed-reactors-in-series model of Eq. (9) was used. Thus, no transport delay was considered, and pure perfect mixing was assumed in each cell constituting the flotation banks.

$$h(t) = \frac{1}{\tau_{PPM}} \exp\left[-\frac{t}{\tau_{PPM}}\right] \tag{8}$$

$$h(t) = \frac{t^{N-1}}{\tau_{\mathrm{PMM}}^{N}\Gamma(N)} \exp\left[-\frac{t}{\tau_{\mathrm{PPM}}}\right] \tag{9}$$

2.3. Modelling Kinetic Responses

From Eq. (2), different $R(t)$ representations can be established, given known residence time and flotation rate distributions. For the former, the measured RTDs were employed, comparing the $R(t)$ modelling results with those obtained under the assumption of pure perfect mixing in each flotation cell. For $f(k)$, three model structures were evaluated, according to Table 2 (García-Zuñiga, 1935; Huber-Panu, 1976; Imaizumi and Inoue, 1963). The Single Rate Constant (SRC) model assumes a single and deterministic rate constant (k_{SRC}). The Rectangular model considers a uniform distribution of rate constants in the range 0 to $k_{\max}$, keeping one rate parameter. The Gamma model has shape (a) and scale (k_0) parameters that allow $f(k)$s from reverse J-shaped distributions ($a < 1$) to normal distributions ($a \to \infty$) to be represented. For the experimental t - R_{data} datasets, the model parameters were again estimated by non-linear regression, solving the minimization problem of Eq. (13).

Table 2. Model structures for the flotation rate distributions.

Model	$f(k)$	k_{mean}	Equation Numbers
SRC (*)	$\delta(k - k_{\mathrm{SRC}})$	k_{SRC}	(10)
Rectangular (**)	$\dfrac{1}{k_{\max}}[\mu(k) - \mu(k - k_{\max})]$	$k_{\max}/2$	(11)
Gamma	$\dfrac{k^{a-1}}{k_0^{a}\Gamma(a)} \exp\left[-\dfrac{k}{k_0}\right]$	$a\,k_0$	(12)

(*) $\delta(k)$ denotes Dirac function; (**) $\mu(k)$ corresponds to the Heaviside function.

$$\begin{aligned} \min \quad & \sum(R_{\mathrm{data}} - R_{\mathrm{model}})^2 \\ & \text{subject to} \\ & 0 \le R_\infty \le 100 \end{aligned} \tag{13}$$

Within Eq. (13) the modelled recoveries R_{model} were obtained from Eq. (2) using an $f(k)$ from Table 2 and the measured $h(t)$s. RTDs under the assumption of pure perfect mixing were also evaluated. Eq. (13) was again implemented in Matlab, using the Optimization Toolbox (The MathWorks, USA).

It should be noted that under pure perfect mixing and by using an SRC or a Rectangular $f(k)$, closed forms for R_{model} are obtained. In all other cases, numerical integration was employed to determine R_{model}.

3. Results and discussion

Fig. 3 shows the reconstruction of the outlet tracer concentration throughout the rougher bank A, using Eq. (3) and the RTD models of Eqs. (5) and (7). The sums of squared residuals (SSR) are presented for comparison purposes. For the first cell [Fig. 3(a)], the best model performance was obtained with two perfect mixers in parallel ($R_{adj}^2 = 0.9861$), including a transport delay (continuous black lines). However, the adjusted coefficient of determination was only slightly greater than that from a single perfect mixer with transport delay ($R_{adj}^2 = 0.9857$). For 3, 5, 7 and 9 cells in series [Fig. 3(b) to 3(e)], the N perfectly-mixed-tanks-in-series model including a transport delay adequately described the experimental RTDs. From all measured and modelled RTDs in the rougher bank A, an average mean residence time per cell of 4.1 ± 0.19 min was obtained, including the 95% confidence interval. Fig. 3 also presents the reconstruction of the outlet tracer concentration (dashed red lines) from RTDs consisting of the actual number of installed machines (i.e., 1, 3, 5, 7 and 9), assuming pure perfect mixing. A residence time per cell of 4.1 min was employed, coinciding with the sample mean value obtained from the measured RTDs. No transport delays were included in this second representation. This RTD description emulates the RTDs typically employed in kinetic characterizations of continuous flotation systems. From Fig. 3, the assumption of perfect mixing with no transport delay led to poor reconstruction of the outlet tracer concentration for five or less cells in series. However, these reconstructions approximately agreed with
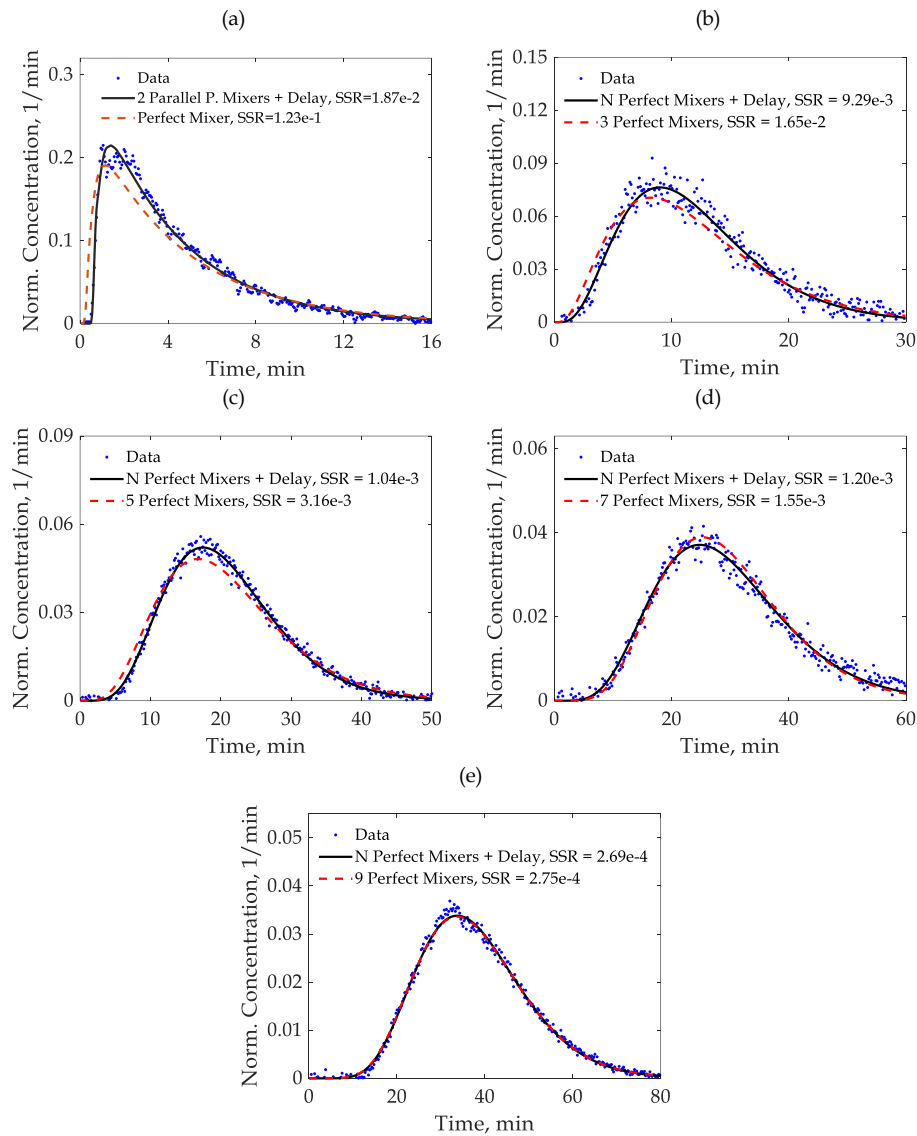
Fig. 3. Output tracer concentrations and model fitting (outlet reconstruction) in mechanical flotation cells, rougher bank A: (a) first cell, (b) three cells in series, (c) five cells in series, (d) seven cells in series, (e) nine cells in series.

those obtained from the parametric deconvolution for 7 and 9 cells in series due to the Central Limit Theorem. For more than 5 flotation cells in series, the RTDs converge to Normal distributions [or Gamma $h(t)$s with $N \rightarrow \infty$], which has been widely observed in industrial circuits (Yianatos *et al.*, 2015). Thus, the assumption of an arrangement of pure perfect mixers (no transport delay) has allowed the RTDs of long flotation banks to be adequately described. However, this representation is only applicable when the actual transport delay is significantly shorter than the cell-by-cell residence time.

Fig. 4 presents the outlet tracer reconstruction for the rougher bank B. In this bank, all flotation cells were characterized. The RTD of the first cell was adequately described by the LSTS model of Eq. (6), with an adjusted coefficient of determination R^2_{adj} = 0.9976. This RTD model was again slightly superior to a perfect mixer including a transport delay (R^2_{adj} = 0.9969). The arrangement of cells in series proved to be consistent with the N perfectly-mixed-tanks-in-series model including a transport delay. From the RTD parameters obtained by Eqs. (3), (6) and (7), a mean residence time of 6.4 ± 0.25 min was observed in single cells of bank B. The reconstruction of the outlet tracer concentration from RTDs described by pure perfect mixers led to poor performances in the first cells [Fig. 4(a) to 4(b)]. Although this reconstruction tended to converge to the deconvolution results for more than 3 cells in series [Fig. 4(d) to (f)], the agreement was less noticeable with respect to that which was observed in bank A

(Fig. 3). In this regard, the lower number of cells in the rougher bank B led to a more gradual convergence to the Central Limit Theorem. From the estimated RTD parameters of the studied rougher banks, the kinetic responses were characterized using Eqs. (1) and (13) and the $f(k)$ model structures of Eqs. (10) to (12).

Fig. 5 compares the model fitting using the estimated RTDs with those assuming pure perfect mixing in each flotation cell of the rougher bank A. The three evaluated kinetic models are presented. Results for the rougher bank B are presented in Appendix A. All modelled recoveries were interpolated by piecewise cubic Hermite polynomials (Kahaner *et al.*, 1988), for better visualization. No appreciable differences in the model fitting were observed between the two studied mixing regimes in all cases. Thus, the differences in the RTDs are compensated by the kinetic parameters, given the flexibility of each model. The same trends were observed in the rougher bank B (Fig. A1, Appendix A). All model structures led to suitable goodness-of-fit, with $R^2_{adj} \geq 0.985$ for the studied mixing regimes in banks A and B. The measured and modelled recoveries shown in Figs. 5 and A1 are presented in Tables B1 and B2 of Appendix B for the studied rougher banks.

Table 3 presents the estimated parameters for each kinetic model and RTD assumptions. The average and median (k_{50}) rate constants are summarized, which correspond to the deterministic values of the SRC model and to $k_{max}/2$ for the Rectangular approach. It should be noted that the Rectangular model
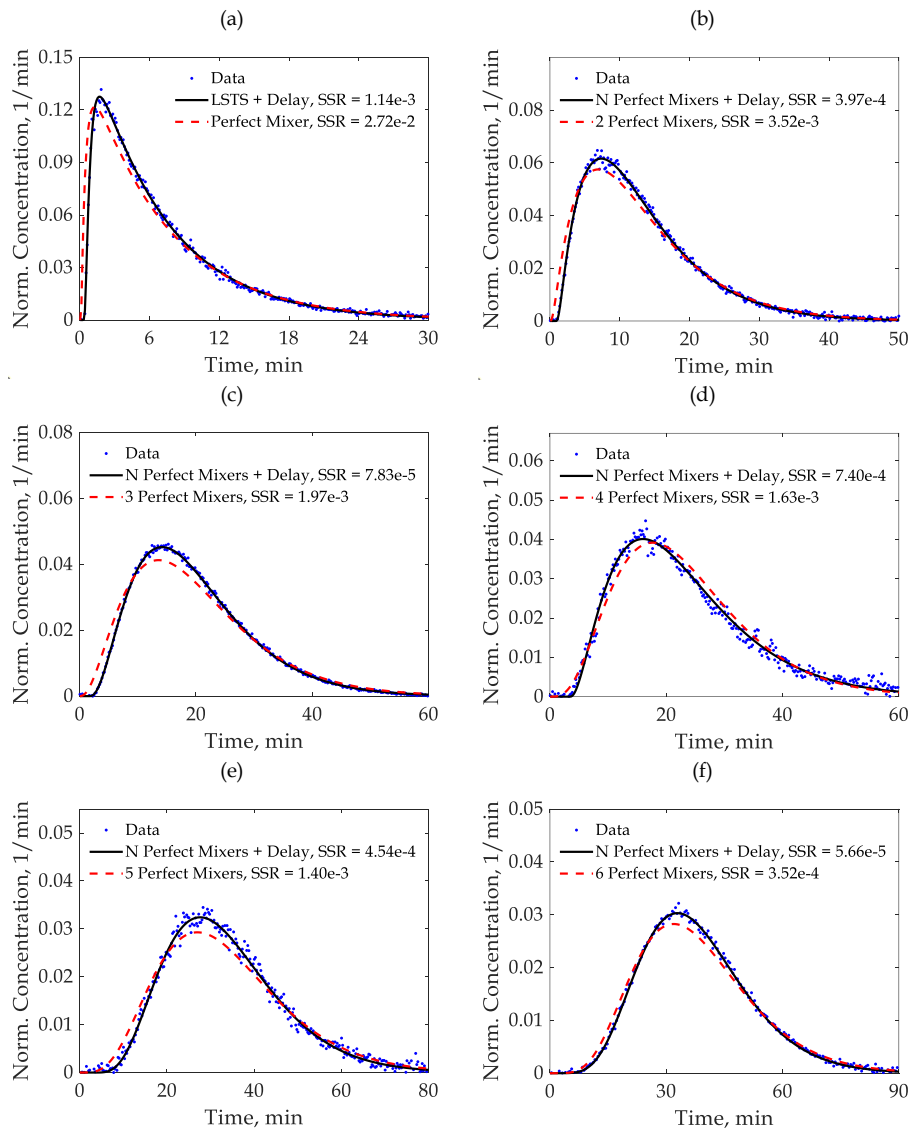

Fig. 4. Output tracer concentrations and model fitting (outlet reconstruction) in mechanical flotation cells, rougher bank B: (a) first cell, (b) two cells in series, (c) three cells in series, (d) four cells in series, (e) five cells in series, (f) six cells in series
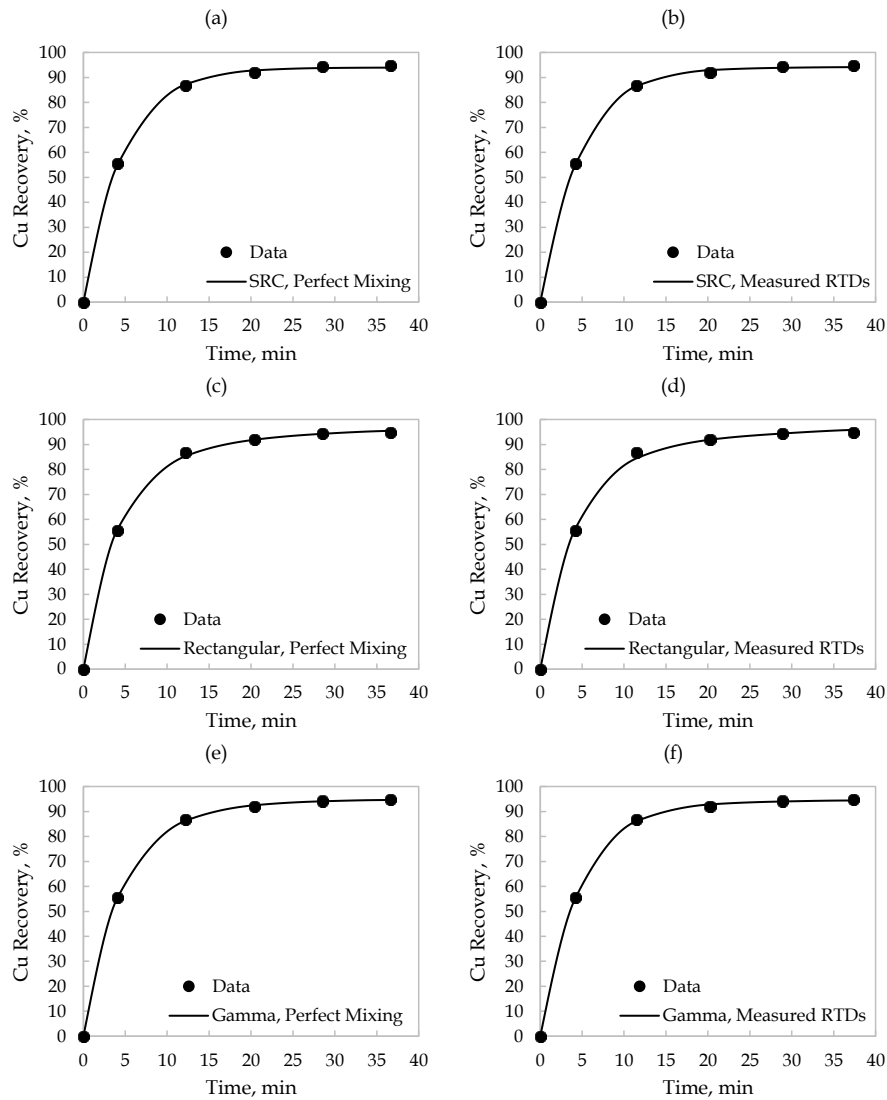
Fig. 5. Kinetic responses and model fitting assuming different mixing regimes in the rougher bank A:
(a) SRC, Perfect mixing; (b) SRC, measured RTDs; (c) Rectangular model, perfect mixing;
(d) Rectangular model, measured RTDs; (e) Gamma model, perfect mixing;
(f) Gamma model, measured RTDs

led to higher R_∞ estimates. This result is caused by the presence of rate constants close to zero in $f(k)$ that distorts the estimation of the non-floating fraction represented by $(100 - R_\infty)$, as discussed by Kelly and Carlson, (1991). From Table 3, the maximum recoveries, and the location indexes (k_{mean} and k_{50}) for the rate constants were moderately changed by the observed RTD deviations with respect to pure perfect mixing in each flotation cell.

Table 3. Kinetic parameters in the rougher banks A and B

Bank	Parameter	SRC		Rectangular		Gamma	
		Perfect Mixing	Measured RTDs	Perfect Mixing	Measured RTDs	Perfect Mixing	Measured RTDs
Bank A	R_∞	94.0	94.2	99.1	100.0	95.0	94.5
	k_{mean}	0.35	0.31	0.42	0.36	0.40	0.32
	k_{50}	0.35	0.31	0.42	0.36	0.37	0.31
Bank B	R_∞	93.3	93.7	98.9	100.0	97.6	96.8
	k_{mean}	0.27	0.24	0.33	0.28	0.38	0.29
	k_{50}	0.27	0.24	0.33	0.28	0.30	0.25

The assumption of pure perfect mixing led to absolute R_∞ differences lower than 1.2% compared to those obtained from the estimated RTDs, as shown in Table 3. The mean and median rate constants presented absolute differences lower than 0.09 1/min. These deviations were not critical, taking the $R(t)$ model fitting of Figs. 5 and A1 (Appendix A) into consideration. Fig. 6 compares the estimated flotation rate distributions from the studied mixing regimes and evaluated kinetic models for the rougher banks A and B. The SRC [Fig. 6(a) and (b)] and Rectangular [Fig. 6(c) and (d)] $f(k)$s presented slight differences by assuming pure perfect mixing with respect to the measured RTDs. As these models are completely defined by the R_∞-k_{SRC} and R_∞-k_{max} pairs, respectively, the $f(k)$ differences are fully explained by the deviations presented in Table 3. The Gamma $f(k)$s [Fig. 6(e) and (f)] proved to be more sensitive to the RTD assumption in the studied kinetic responses, due to their higher flexibility. Thus, the shapes of these estimated flotation rate distributions were affected by the mixing regimes. Although the differences in the $f(k)$ shapes were also moderate, the identification of fast- and slow-floating components from high and low k percentiles as reported by Vinnett *et al.*, (2022) may be affected by the assumed RTDs. Kinetic characterizations only dependent on the R_∞-k_{mean} or R_∞-k_{50} pairs and model fitting are not significantly affected by the perfect mixing assumption, as shown in Table 3, Fig. 5 and Fig. A1 (Appendix A). This result is applicable under moderate deviations with respect to perfect mixing, as shown in Figs. 3(a) and 4(a). Further developments are being made to expand these findings to industrial flotation circuits subject to significant bypass throughout the banks. Fractioning kinetic responses by-size or other particle properties will allow the impact of mixing assumptions on the identification of floating-components to be evaluated.
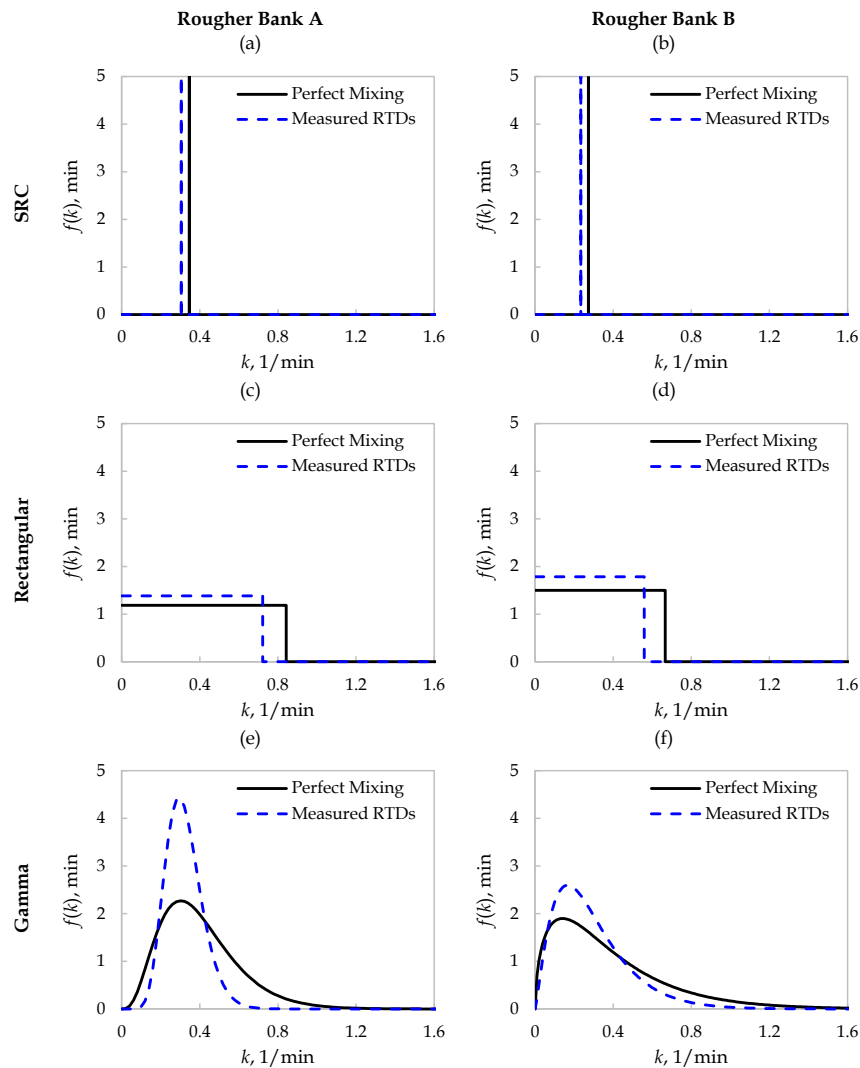

Fig. 6. Estimations of the flotation rate distributions in the rougher banks A and B for the studied mixing regimes. SRC: (a) bank A; (b) bank B. Rectangular model (c) bank A; (d) bank B. Gamma model (e) bank A; (f) bank B

4. Conclusions

Hydrodynamic and metallurgical surveys were conducted in two industrial flotation banks to characterize the residence time distributions and kinetic responses in continuous systems. A comparison of the estimated kinetic parameters was carried out, considering the measured RTDs and assuming pure perfect mixing in each flotation cell. From the analysis, the following results were obtained:

1. Pure perfect mixing fails to accurately fit outlet tracer concentrations for less than 5 cells in series. However, this RTD description agrees as the number of cells in series increases, due to the Central Limit Theorem.
2. The $f(k)$ flexibilities allowed the perfect mixing assumption to be compensated. As a result, similar model fitting was obtained for all kinetic responses from the measured and assumed RTDs.
3. No significant differences in R_∞, k_{mean} and k_{50} were observed when characterizing the kinetic responses from the measured and assumed (pure perfect mixing) RTDs.
4. The flexibility of the Gamma model led to moderate changes in the $f(k)$ under the studied mixing regimes. These deviations may hinder the identification of floating components from $f(k)$ percentiles when assuming pure perfect mixing.
5. Kinetic characterizations based on model fitting, and on R_∞-k_{mean} or R_∞-k_{50} estimations have low sensitivity to the perfect mixing assumption under moderate deviations with respect to this regime.

From the studied datasets, the kinetic parameters (R_∞-k_{mean}-k_{50}) presented low sensitivity to the assumption of perfect mixing in continuous flotation systems. This result is applicable to flotation banks with moderate deviations regarding this regime in single cells. Caution is advised in the use of these findings when the residence time distributions present significant bypass throughout the banks.

Appendix A

Fig. A1 presents the model fitting using the estimated RTDs and assuming pure perfect mixing in each flotation cell of the rougher bank B. Similar trends to those observed in the rougher bank A (Fig. 5) are observed.
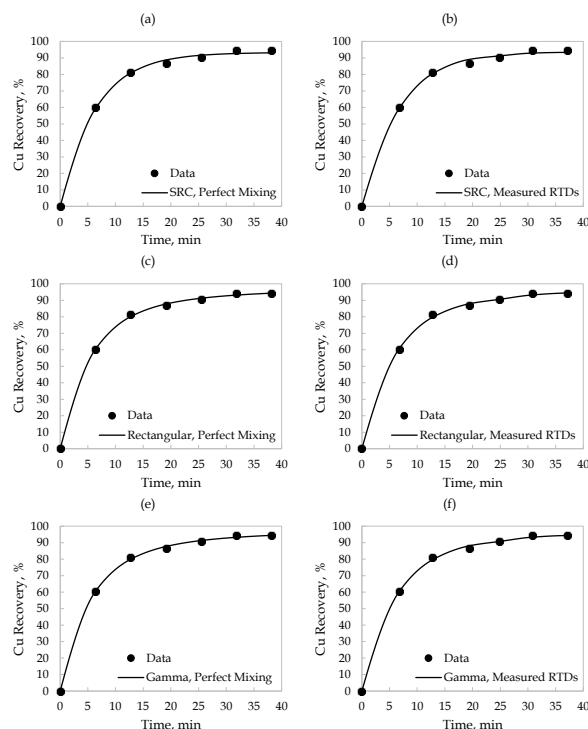

Fig. A1. Kinetic responses and model fitting assuming different mixing regimes in the rougher bank B:
(a) SRC, Perfect mixing; (b) SRC, measured RTDs; (c) Rectangular model, perfect mixing; (d) Rectangular model, measured RTDs; (e) Gamma model, perfect mixing; (f) Gamma model, measured RTDs

Appendix B

Tables B1 and B2 detail the measured and modelled Cu recoveries in the rougher banks A and B, respectively, considering all kinetic models, and the measured and assumed mixing regimes.

Table B1. Measured and modelled recoveries in the rougher bank A

Cell Number	Measured Cu Recovery (%)	Modelled Cu Recoveries (%)					
		Assumed Perfect Mixing			Measured RTDs		
		SRC	Rectangular	Gamma	SRC	Rectangular	Gamma
1	55.5	55.0	56.1	55.5	55.4	56.6	55.6
3	86.7	87.3	85.4	86.3	86.6	84.5	86.2
5	91.9	92.8	91.9	92.5	93.0	91.9	92.8
7	94.2	93.8	94.3	94.1	93.9	94.4	94.0
9	94.7	93.9	95.5	94.6	94.2	95.9	94.4

Table B2. Measured and modelled recoveries in the rougher bank B

Cell Number	Measured Cu Recovery (%)	Modelled Cu Recoveries (%)					
		Assumed Perfect Mixing			Measured RTDs		
		SRC	Rectangular	Gamma	SRC	Rectangular	Gamma
1	60.1	59.3	60.4	60.5	59.7	60.9	60.6
2	81.2	80.9	80.1	79.9	80.4	79.6	79.6
3	86.6	88.8	87.7	87.6	89.1	87.9	88.2
4	90.5	91.7	91.2	91.3	91.2	90.5	90.8
5	94.2	92.7	93.1	93.2	92.9	93.2	93.4
6	94.2	93.1	94.3	94.4	93.3	94.4	94.3

Acknowledgments

References

ABKHOSHK, E., KOR, M., REZAI, B., 2010. *A study on the effect of particle size on coal flotation kinetics using fuzzy logic*, Expert Syst. Appl. 37(7), 5201-5207.

AI, G., YANG, X., LI, X., 2017. *Flotation characteristics and flotation kinetics of fine wolframite*, Powder Technol. 305, 377-381.

BU, X., XIE, G., PENG, Y., 2017a. *Interaction of fine, medium, and coarse particles in coal fines flotation*, Energy Sources A: Recovery Util. Environ. Eff. 39(12), 1276-1282.

BU, X., XIE, G., PENG, Y., GE, L., NI, C., 2017b. *Kinetics of flotation. order of process, rate constant distribution and ultimate recovery*. Physicochem. Probl. Miner. Process. 53, 342-365.

BOEREE, C.R., 2014. *Up-scaling of froth flotation equipment*. M. Sc. Thesis. Delft University of Technology.

DOWLING, E.C., KLIMPEL, R.R., APLAN, F.F., 1985. *Model discrimination in the flotation of a porphyry copper ore*. Miner. Metall. Process. 2, 87-101.

EK, C., 1992. *Flotation Kinetics*, Innovations in Flotation Technology. Springer Dordrecht, The Netherlands, 183-210.

GARCIA-ZUÑIGA, H., 1935. *La recuperación por flotación es una función exponencial del tiempo*. Boletín Minero, Sociedad Nacional de Minería 47, 83-86.

GHARAI, M., VENUGOPAL, R., 2016. *Modeling of flotation process – an overview of different approaches*. Miner. Process. Extr. Metall. Rev., 37(2), 120-133.

HUBER-PANU, I., ENE-DANALACHE, E., COJOCARIU, D.G., 1976. *Mathematical models of batch and continuous flotation*. Flotation–A. M. Gaudin Memorial, 675-724.

IMAIZUMI, T., INOUE, T., 1963. *Kinetic considerations of froth flotation*. Proceedings of the 6th International Mineral Processing Congress, Cannes. 581–593.

KAHANER, D., MOLER, C.B., NASH, S., FORSYTHE, G.E., 1988. *Numerical Methods and Software*. Prentice Hall, Englewood Cliffs, N.J.

KELLY, E.G., CARLSON, C.E., 1991. *Two flotation models: resolution of a conflict*. Miner. Eng. 4 (12), 1333–1338.

YEKELER, M., SÖNMEZ, İ., 1997. *Effect of the hydrophobic fraction and particle size in the collectorless column flotation kinetics*, Colloids Surf. A Physicochem. Eng. Asp. 121(1), 1997, 9-13.

POLAT, M., CHANDER, S., 2000. *First-order flotation kinetics models and methods for estimation of the true distribution of flotation rate constants*, Int. J. Miner. Process. 58(1-4), 145-166.

QAREDAQI, M., SHIRAZI, H.H.A., ABDOLLAHI, H., 2012. Comparison of Yianatos and traditional methods to determine kinetic rate constants of different size fractions in industrial rougher cells. Int. J. Miner. Process. 106, 65-69.

SALDAÑA, M., NEIRA, P., FLORES, V., MORAGA, C., ROBLES, P., SALAZAR, I. 2021. *Analysis of the Dynamics of Rougher Cells on the Basis of Phenomenological Models and Discrete Event Simulation Framework*. Metals 11(9), 1454.

SCHUHMANN JR, R., 1942. *Flotation Kinetics. I. Methods for steady-state study of flotation problems*. J. Phys. Chem. 46, 891-902.

VÉDRINE, H., BROUSSAUD, A., CONIL, P., DE MATOS, C., 1991. *Modelling the Flotation Kinetics of a Polymetallic Sulphide Ore*, SME Annual Meeting, Denver, Colorado, USA.

VINNETT, L., YIANATOS, J., FLORES, S., 2016. *On the mineral recovery estimation in* Cu/Mo *flotation plants*. Miner. Metall. Process. 33, 97-106.

VINNETT L, WATERS K.E., 2020. *Representation of Kinetics Models in Batch Flotation as Distributed First-Order Reactions*. Minerals 10(10), 913.

VINNETT, L., GRAMMATIKOPOULOS, T., EL-MENSHAWY, A.H., WATERS, K.E., 2022. *Justifying size-by-size flotation rate distributions from size-by-association kinetic responses*, Powder Technol. 395, 168-182.

WILLS, B., NAPIER-MUNN, T., 2006. *Wills' Mineral Processing Technology: An Introduction to the Practical Aspects of Ore Treatment and Mineral Recovery*. (7th ed.), Butterworth-Heinemann, Oxford.

WOODBURN, E.T., LOVEDAY, B.K., 1965. *The effect of variable residence time on the performance of a flotation system*. Journal of the Southern African Institute of Mining and Metallurgy 65, 612-628.

YIANATOS, J., BERGH, L., VINNETT, L., PANIRE, I., DIAZ, F., 2015. *Modelling of residence time distribution of liquid and solid in mechanical flotation cells*, Miner. Eng. 78, 69-73.